Draft version November 12, 2024
Typeset using LaTeX **preprint2** style in AASTeX631

arXiv:2411.07080v1 [astro-ph.GA] 11 Nov 2024

Machine Learning Approach for Estimating Magnetic Field Strength in Galaxy Clusters from Synchrotron Emission

Jiyao Zhang,[1] Yue Hu*,[2] and Alex Lazarian[3]

[1] *Department of Mathematics, University of Pennsylvania, Philadelphia, PA 19104, USA*
[2] *Institute for Advanced Study, 1 Einstein Drive, Princeton, NJ 08540, USA*
[3] *Department of Astronomy, University of Wisconsin-Madison, Madison, WI 53706, USA*

ABSTRACT

Magnetic fields play a crucial role in various astrophysical processes within the intracluster medium, including heat conduction, cosmic ray acceleration, and the generation of synchrotron radiation. However, measuring magnetic field strength is typically challenging due to the limited availability of Faraday Rotation Measure sources. To address the challenge, we propose a novel method that employs Convolutional Neural Networks (CNNs) alongside synchrotron emission observations to estimate magnetic field strengths in galaxy clusters. Our CNN model is trained on either Magnetohydrodynamic (MHD) turbulence simulations or MHD galaxy cluster simulations, which incorporate complex dynamics such as cluster mergers and sloshing motions. The results demonstrate that CNNs can effectively estimate magnetic field strengths with median uncertainties of approximately 0.22μG, 0.01μG, and 0.1μG for $\beta = 100$, 200, and 500 conditions, respectively. Additionally, we have confirmed that our CNN model remains robust against noise and variations in viewing angles with sufficient training, ensuring reliable performance under a wide range of observational conditions. We compare the CNN approach with the traditional magnetic field strength estimates method that assumes equipartition between cosmic ray electron energy and magnetic field energy. Unlike the equipartition method, this CNN approach does not rely on the equipartition assumption, offering a new perspective for comparing traditional estimates and enhancing our understanding of cosmic ray acceleration mechanisms.

Keywords: Galaxy clusters (584) —Intracluster medium (858) — Magnetic fields (994) — Convolutional neural networks (1938) — Radio astronomy (1338)

1. INTRODUCTION

Magnetic fields play a pivotal role across a vast range of astrophysical scales, influencing phenomena from micro-scale cosmic ray transport and acceleration (Jokipii 1966; Bell 1978a; Yan & Lazarian 2002; Bell 2004; Bykov et al. 2012; Caprioli & Spitkovsky 2014; Bonafede et al. 2014; Xu & Lazarian 2022; Xu 2022; Hu et al. 2022b), small-scale star formation (Mestel 1965; Mac Low & Klessen 2004; McKee & Ostriker 2007; Lazarian et al. 2012; Federrath & Klessen 2012; Burkhart & Mocz 2019; Hu et al. 2021; Alina et al. 2022; Hu & Lazarian 2023), to large-scale galaxy cluster evolution (Carilli & Taylor 2002; Govoni & Feretti 2004; Brunetti & Jones 2014; Stuardi et al. 2021; Hu et al. 2024b). However, despite its significance, studying magnetic fields, particularly in the Intracluster Medium (ICM), remains notoriously challenging.

Synchrotron emission and polarization serve as key diagnostic tools for estimating the equipartition magnetic field strength and for determining the magnetic field's orientation within the plane-of-the-sky (POS), respectively (Rybicki & Lightman 1986; Condon 1992; Chevalier & Luo 1994; Arshakian et al. 2009; Planck Collaboration et al. 2016; Zhang et al. 2019a; Hu et al. 2022a). These studies have significantly advanced our understanding, indicating that the typical magnetic field strength in the ICM is at the microgauss (μG) level, with magnetic field correlations extending from a few kpc to hundreds of kpc (Govoni & Feretti 2004; Beck & Krause 2005; Brunetti & Jones 2014; Stuardi et al. 2021). However, the assumption of equipartition be-

jiyaoz@sas.upenn.edu; yuehu@ias.edu; alazarian@facstaff.wisc.edu; *NASA Hubble Fellow

tween cosmic ray electrons and magnetic fields is poorly justified (Beck & Krause 2005), and the utility of polarized synchrotron emission is often limited by depolarization effects. These include Faraday depolarization, which results from the presence of thermal electrons and turbulent magnetic fields along the line-of-sight (LOS), and beam depolarization, which arises from a randomized magnetic field distribution within the POS. Such depolarization challenges the use of this method in extensive cluster regions, such as radio halos (Govoni & Feretti 2004; Stuardi et al. 2021; Hu et al. 2024b). On the other hand, the Faraday Rotation Measure (RM), derived from the rotation of a polarized source's angle with wavelength, provides insights into the LOS magnetic field, weighted by the thermal electron density (Murgia et al. 2004; Melrose 2010; Brentjens & De Bruyn 2005). Nevertheless, this technique is often limited by the scarcity of radiation sources with well-defined properties, complicating detailed studies (Andrecut et al. 2011; Johnson et al. 2020).

Most astrophysical fluids are both magnetized and turbulent. Magnetohydrodynamic (MHD) turbulence is anisotropic (Goldreich & Sridhar 1995; Lazarian & Vishniac 1999) and this induces the statistical anisotropy of the synchrotron emission (Lazarian & Pogosyan 2012). The elongation direction can be used to probe the POS magnetic field orientation. Hu & Lazarian (2024a,b) further noticed that this anisotropy not only reflects the POS magnetic field but is also affected by the projection effect along the LOS, and the medium's level of magnetization, defined as M_A^{-1}. Here $M_A = \delta v_{\rm inj}\sqrt{4\pi\rho}/B$ is the Alfvén Mach number, with $\delta v_{\rm inj}$ being turbulence injection velocity, ρ mass density, and B magnetic field strength. Hu & Lazarian (2024a) introduced the use of Convolutional Neural Networks (CNNs; LeCun et al. 1998) to extract the observed anisotropy in synchrotron emissions and thereby facilitate the measurement of 3D magnetic fields.

In this paper, we aim to extend the CNN approach to estimate magnetic field strength using synchrotron emission. Hu & Lazarian (2024a) primarily retrieved the medium's magnetization rather than its magnetic field strength. Schmaltz et al. (2024) extend the CNN approach to estimate the kinetic energy of turbulence, characterized by the sonic Mach number $M_s = \delta v_{\rm inj}/c_s$, where c_s is the sound speed. The product $M_A^{-1}M_s$ thus gives the ratio of magnetic field energy and thermal kinetic energy. It suggests that the two Mach numbers contain information on magnetic field strength (Lazarian et al. 2022, 2024). Therefore, we aim to develop a CNN model to extract the strength information directly. Importantly, this approach does not assume equipartition between cosmic ray electrons and magnetic fields, allowing for a comparison with traditional equipartition estimates and providing insights into the cosmic ray acceleration mechanism.

On the other side, the training of CNNs in Hu & Lazarian (2024a) was based on simulations of MHD turbulence and did not include complexities like cluster mergers, sloshing motions, or cooling and heating dynamics found in galaxy clusters, which could affect the validity of their model under realistic cluster conditions. In this work, we train the CNN model with either MHD turbulence simulations or numerical MHD galaxy cluster simulations from the Galaxy Cluster Merger Catalog (ZuHone et al. 2011, 2018). These cluster simulations feature three different initial plasma compressibilities ($\beta = 100, 200, 500$) and include a dark matter subcluster passing near the center of a main cool-core cluster, mimicking systems like Perseus and Abell 2029.

This paper is structured as follows: in § 2 we discuss the theoretical consideration that the morphology of synchrotron emission observation contains information on magnetic field strength. In § 3, we detail the MHD turbulence and galaxy cluster simulations, as well as the mock synchrotron observation, utilized in our study. § 4 briefly revisits the architecture of our CNNs and our training strategies. In § 5, we present the results derived from our numerical testing, offering insights into the efficacy and accuracy of the CNN model. § 6 delves into discussions surrounding the uncertainties and prospects of employing CNNs for observational analysis. We conclude with a summary of our findings in § 7.

2. THEORETICAL CONSIDERATION

To illustrate the physics behind the CNN approach for estimating the magnetic field strength, we start with a clean system considering only the MHD turbulence.

2.1. *Magnetic field strength is imprinted in M_A and M_s*

Alfvén Mach number M_A and sonic Mach number M_s are two important parameters in characterizing the properties of MHD turbulence. The two Mach numbers are defined as:

$$M_A = \frac{\delta v_{\rm inj}}{v_A} = \frac{\delta v_{\rm inj}}{B}\sqrt{4\pi\rho}, \tag{1}$$

$$M_s = \frac{\delta v_{\rm inj}}{c_s}, \tag{2}$$

where v_A is the Alfvén speed. The squared M_A reflects the relative importance of turbulent kinetic energy and magnetic field energy, while the squared M_s characterizes the ratio of turbulent kinetic energy and thermal kinetic energy.

Combining two Mach numbers, the magnetic field strength B can be expressed as:

$$B = c_s\sqrt{4\pi\rho}M_s M_A^{-1}, \tag{3}$$

which suggests that if M_A and M_s are known, one could determine magnetic field strength from observations. This approach, denoted as MM2, was originally suggested and elaborated by Lazarian et al. (2022, 2024).

2.2. *Estimating M_A with CNN*

Estimating M_A with CNN and synchrotron emission is proposed in Hu & Lazarian (2024a). For a turbulent eddy at scale l, we can decompose its scale into the parallel $l_\parallel$ and perpendicular $l_\perp$ components with respect to the local magnetic field. Turbulent energy cascades predominantly in the perpendicular direction due to fast turbulent reconnection, which minimizes resistance in that direction. Eventually, this cascade achieves a state of "critical balance" with the Alfvén wave, which propagates along the parallel direction. This balance can be expressed as:

$$\delta v_{l_\perp} l_\perp^{-1} \sim v_A l_\parallel^{-1}, \tag{4}$$

where $\delta v_{l_\perp}$ denotes the velocity fluctuations at the perpendicular scale $l_\perp$. Additionally, in the regime of strong turbulence, the cascade follows a Kolmogorov-type scaling relation (Xu 2019):

$$\delta v_{l_\perp} = (\frac{l_\perp}{L_{\rm inj}})^{1/3} v_{\rm inj} M_A^{1/3}, \tag{5}$$

where $L_{\rm inj}$ is the injection scale $L_{\rm inj}$. Combing Eqs. 4 and 5, one can get the scale-dependent anisotropy scaling (Lazarian & Vishniac 1999)[1]:

$$l_\parallel = L_{\rm inj}(\frac{l_\perp}{L_{\rm inj}})^{\frac{2}{3}} M_A^{-4/3}, \tag{6}$$

which suggests that the ratio of $l_\parallel/l_\perp$ depends on M_A. A higher magnetization leads to a larger $l_\parallel/l_\perp$ ratio, while weaker magnetization decreases this ratio.

Eq. 6 provides the scaling relation for velocity fluctuations. The relationships for magnetic field fluctuations δB_l can also be derived using the linearized continuity and induction equations, considering the components as a sum of their mean and fluctuating parts (see Hu & Lazarian 2024a for details):

$$\delta B_l = \delta v_l \frac{B}{v_A}\mathcal{F}^{-1}(|\hat{\boldsymbol{B}} \times \hat{\boldsymbol{\xi}}|), \tag{7}$$

where $\hat{\boldsymbol{k}}$ and $\hat{\boldsymbol{\xi}}$ represent the unit wavevector and displacement vector, respectively. $\mathcal{F}^{-1}$ denotes the inverse Fourier transform. Since fluctuations in synchrotron emission intensity primarily arise from magnetic field fluctuations (see Eq. 8), their statistical properties are governed by MHD turbulence. Consequently, the aspect ratio of an observed synchrotron structure correlates with M_A (see Fig. 1).

However, the observed synchrotron intensity is projected onto the POS. The projection alters the $l_\parallel/l_\perp$ ratio. This introduces a degeneracy, as both LOS projection and changes in M_A can affect the observed anisotropy. To resolve this degeneracy, additional information on the structure's morphological curvature is required. Strong magnetic field fluctuations, i.e., large M_A, result in significantly curved magnetic field lines (see Fig. 1). These fluctuations are naturally mirrored in synchrotron observations and their morphological curvature. This provides key information for estimating M_A. Hu & Lazarian (2024a) proposed utilizing CNNs to extract the information and ultimately estimate M_A from synchrotron emission data.

2.3. *Estimating M_s with CNN*

In addition to estimating M_A, Schmaltz et al. (2024, in prep.) extend the CNN to measure M_s. The relationship between M_s, density fluctuations, and magnetic field fluctuations is well-established. In media with high M_s, shocks play a more dominant role, and the small-scale, high-amplitude fluctuations produced by these shocks are imprinted in synchrotron intensity maps. This indicates that variations in M_s are distinctly reflected in the intensity maps, providing a physical foundation for extracting M_s information from synchrotron observations using CNNs. For further details, we refer readers to Schmaltz et al. (2024) .

To summarize, the observed synchrotron emission map contains detailed information on M_A and M_s. Especially, the morphological features, including the aspect ratio, curvature, and small-scale shock structures, in the synchrotron map are sensitive to either M_A or M_s. The combination of M_A and M_s, on the other hand, correlates with the magnetic field strength (see Eq. 3). In Appendix A, we provide a test of the CNN's performance in estimating the magnetic field strength using MHD turbulence simulations. In a complicated system of galaxy clusters, fluctuations in synchrotron intensity

[1] This scaling relation is valid for sub-Alfvénic turbulence with $M_A \leq 1$. For super-Alfvénic scenarios where $M_A \gg 1$, turbulence cascades energy from larger injection scales down to smaller scales and progressively diminishes turbulent velocity. Assuming Kolmogorov turbulence, the magnetic field's energy approaches that of turbulence (i.e., the M_A is unity) at the transition scale $l_A = L_{\rm inj}/M_A^3$, below which the magnetic field's role becomes important and the anisotropy can be observed (Lazarian 2006). l_A is estimated to be 1 - 60 kpc in ICM (Hu et al. 2024b).

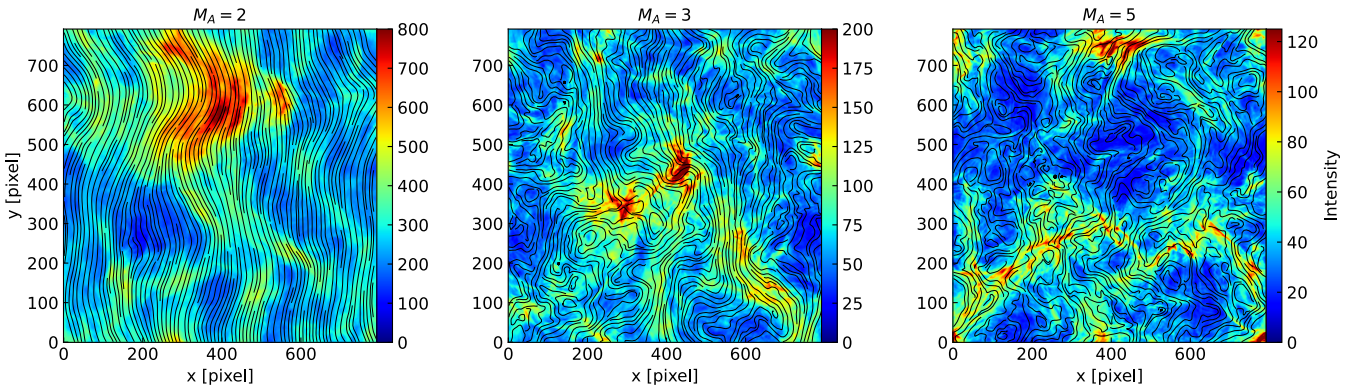

Figure 1. Maps of synchrotron emission intensity generated from MHD turbulence simulations. Three different initial $M_A = 2$ (left), $M_A = 3$ (middle), and $M_A = 5$ (right) are presented. The black streamlines represent the density-weighted POS magnetic field orientation.

Simulation Names	Initial β	Resolution	Minimum B-strength	Maximum B-strength
beta100_310	100	2 kpc / pixel	0.010 μG	5.57 μG
beta200_310	200	2 kpc / pixel	0.002 μG	4.75 μG
beta500_310	500	2 kpc / pixel	0.004 μG	3.13 μG

Table 1. Overview of galaxy cluster simulations used in this work. We use the snapshots of the clusters at 3.1 Gyr. Three different initial plasma β are included.

are not only induced by MHD turbulence. However, the changes in magnetic field strength, thus, are also expected to be imprinted in the synchrotron map, as shown in § 5.

3. NUMERICAL SIMULATIONS

3.1. *MHD simulations of galaxy cluster*

The numerical simulations used in this research come from ZuHone et al. (2011). They simulated idealized binary galaxy cluster mergers by solving ideal MHD equations and setting up a dark matter subcluster passing near the center, mimicking typical conditions of cool-core clusters and producing sloshing and turbulent gas motions in cluster cores. The simulations were generated from the parallel hydrodynamics/N-body astrophysical simulation code FLASH 3 (Fryxell et al. 2000; Dubey et al. 2009). Using a directionally unsplit staggered mesh (USM) algorithm which guarantees that the evolved magnetic field satisfies the divergence-free condition (Evans & Hawley 1988).

Three distinct initial conditions were tested, characterized by different plasma compressibilities: $\beta = 100, 200, 500$, where $\beta = p_{\rm th}/p_B$. Here, $p_{\rm th}$ and p_B represent the gas thermal pressure and magnetic field pressure, respectively. These conditions encompass a range of initial magnetic field strengths, as detailed in Tab. 1. The simulated galaxy cluster spans a length scale of 1 Mpc and is discretized into a 512^3 grid, achieving a resolution of approximately 2 kpc per pixel. For additional details regarding the setup of these simulations, we refer readers to ZuHone et al. (2011).

3.2. *Synthetic synchtron emission*

To generate synthetic synchrotron observations from our simulations, we use the density field $\rho(\boldsymbol{x})$ and the magnetic field $\boldsymbol{B}(\boldsymbol{x})$. The calculations for synchrotron intensity $I(\boldsymbol{X})$ is based on (Rybicki & Lightman 1986; Pacholczyk 1970; Lee et al. 2016):

$$I(\boldsymbol{X}) \propto \int dz\ n_{e,r}(B_x^2 + B_y^2)^{\frac{\gamma-3}{4}}(B_x^2 + B_y^2), \tag{8}$$

where $\boldsymbol{X} = (x, y)$ and $\boldsymbol{x} = (x, y, z)$ represent spatial coordinates. $n_{e,r}(\boldsymbol{x}) = \rho(\boldsymbol{x})$ is the relativistic electron number density, and γ denotes the spectral index of the electron energy distribution E:

$$N(E)dE = N_0 E^{-\gamma} dE, \tag{9}$$

with $N(E)$ representing the electron number density per unit energy interval dE. The pre-factor N_0 is derived by integrating Eq. 9 to obtain the total electron number density. Given the relative insensitivity of synchrotron emission to variations in the electron energy distribution's spectral index, as noted by Lazarian & Pogosyan (2012); Zhang et al. (2019b), we assume a homogeneous and isotropic electron energy distribution with a spectral index $\gamma = 3$. Other constant factors at a given γ are not explicitly detailed in Eq. 8, as they do not alter the characteristics of the synchrotron intensity fluctuations.

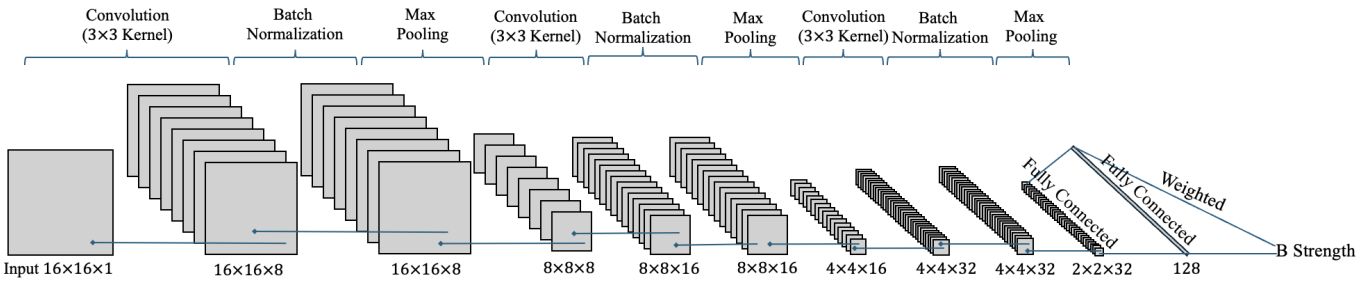

Figure 2. Architecture of the CNN-model. The input image is a 16 × 16 pixel map cropped from the synchrotron intensity map. The network outputs a scalar - the prediction of magnetic field strength. Modified from Hu et al. (2024a).

4. METHODOLOGY

4.1. *CNN Model*

The CNN model employed in this study follows the architecture outlined by Hu et al. (2024a), specifically designed to interpret the 3D magnetic fields from synchrotron emission maps. The detailed architecture of this model is illustrated in Fig. 2, showcasing a multi-layered approach that includes convolutional layers, batch normalization layers, and max pooling layers.

Convolutional Layers: These layers utilize various convolution kernels to separate and extract local features from the input images. Each convolutional layer aims to identify distinct patterns within the data, which are crucial for understanding the underlying magnetic field structures.

Batch Normalization Layers: Following each convolutional layer, a batch normalization layer is implemented. This layer normalizes the activations of the previous layer at each batch, i.e., it applies a transformation that maintains the mean output close to 0 and the output standard deviation close to 1. This normalization helps to expedite convergence and enhance learning stability during network training via backpropagation (Ioffe & Szegedy 2015).

Max Pooling Layers: A common variant in the pooling layers is the Max Pooling Layer, which reduces the spatial size of the input images, making the detection of features invariant to scale and orientation changes more efficient (Scherer et al. 2010). This layer operates by selecting the maximum value from a specified window of neurons and outputs this value, effectively reducing the dimensionality of the input feature map while retaining the most critical feature information.

After several cycles of convolution, normalization, and pooling, the dimensions of the input images are significantly reduced, yet enriched with important local features. These processed images are then flattened into a 1D vector containing the extracted features. This vector feeds into the fully connected layers, which perform the final analysis to predict the strength of the magnetic field based on the learned features. A detailed discussion of each layer's function is given in Hu et al. (2024a).

4.2. *Training Strategy*

The CNN architecture described has demonstrated its effectiveness in tracing 3D magnetic fields using synchrotron observations. The model's trainable parameters are optimized using a typical conventional neural network training approach. The optimization process is guided by the Mean-Squared Error (MSE) of the predicted magnetic field strength distribution against the actual field strength, which serves as the loss function for backpropagation. This methodology is based on the foundational principles laid out by (Rumelhart et al. 1986), which emphasize the importance of efficient error reduction through iterative learning.

To further enhance the model's generalization capabilities and ensure robust performance on unseen data, we have implemented a data augmentation strategy during the training phase (Takahashi et al. 2020). This strategy involves subjecting the input synchrotron images to random cropping, reducing them to patches of 16×16 pixels. Each of these patches is then rotated by a random angle before being fed into the CNN. This process of cropping and rotating not only introduces variability but also injects randomness into the training dataset (van Dyk & Meng 2001; Larochelle et al. 2007). Such augmentation techniques are crucial for helping the network learn to generalize effectively from the training data to unseen data, thereby boosting the model's predictive accuracy and robustness.

5. RESULTS

5.1. *Synchrotron emission's morphological correlation with magnetic field strength*

The morphology observed in synchrotron emission maps is intricately influenced by both the distribution of relativistic electron number density and the magnetic field projected onto the POS (see Eq. 8). A stronger magnetic field enhances magnetic pressure, compressing the gas or particles and leading to synchrotron

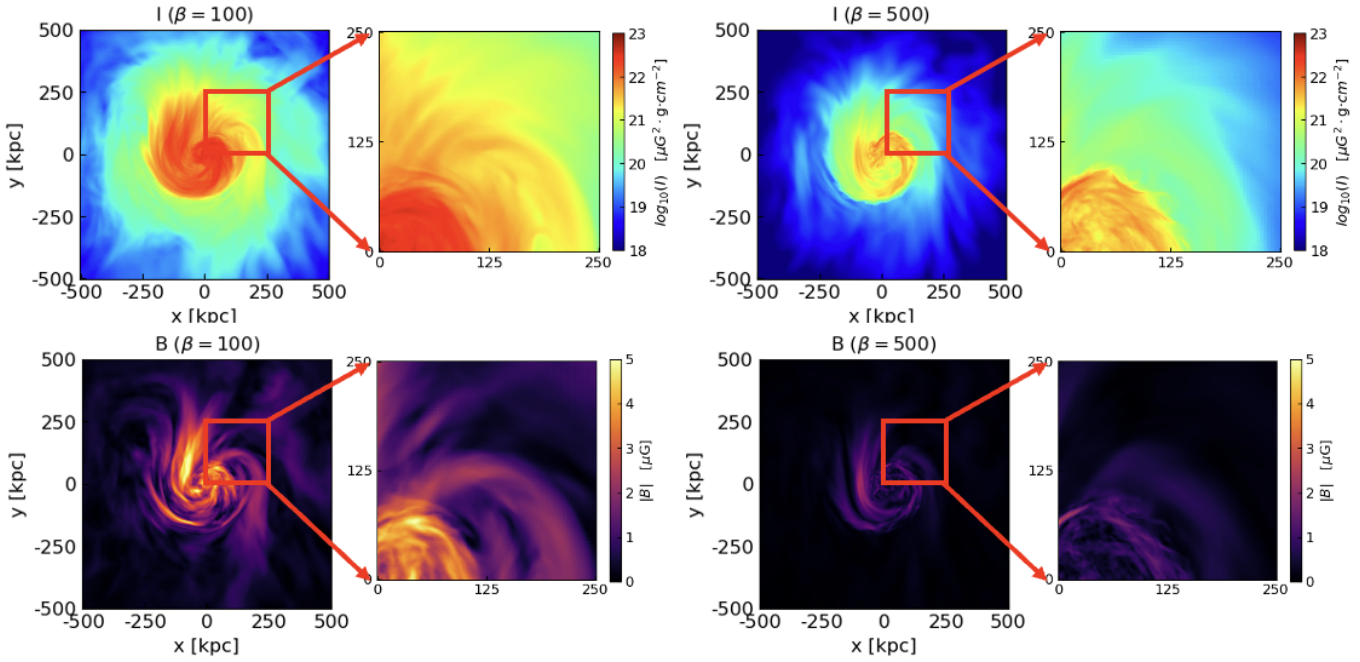

Figure 3. Maps of synchrotron emission intensity (top) and the corresponding project mass-weighted magnetic field strength (bottom). Two different initial $\beta = 100$ (left) and $\beta = 500$ (right) are presented. The zoom-in image on the right of each panel shows the structural differences in synchrotron intensity maps due to different initial β.

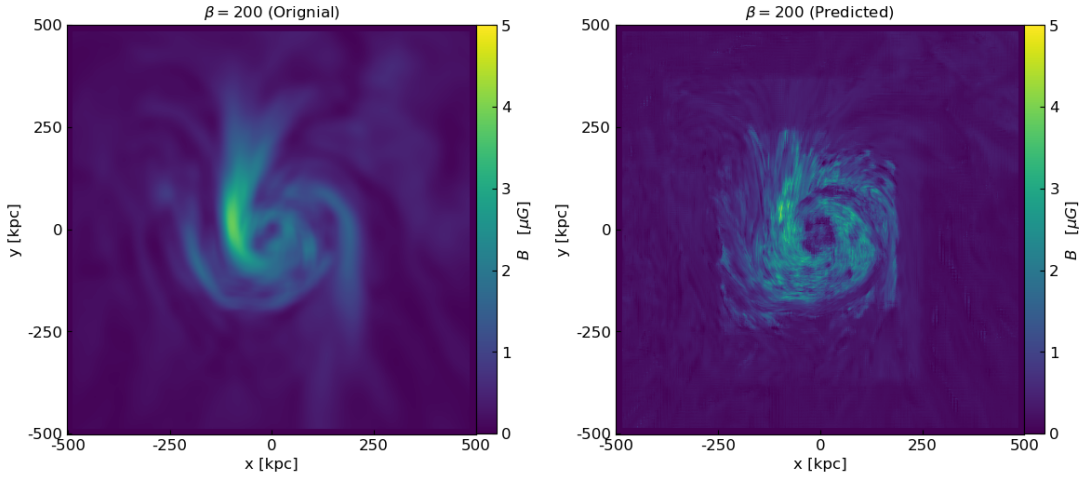

Figure 4. A comparison of the magnetic field strength predicted by CNN (right panel) and the actual mass-weighted magnetic field strength (left panel) in the $\beta = 200$ simulation.

structures that appear less clumped compared to those formed in regions with weaker magnetic fields. Moreover, magnetic-field-dependent instabilities, such as the magnetorotational instability (MRI; Nipoti et al. 2015) and the magneto-thermal instability (MTI; Perrone & Latter 2022), generate turbulence in galaxy clusters. This turbulence further affects the distribution of gas density and magnetic field fluctuations, which in turn shape the observed synchrotron structures, providing insights into the POS magnetic field strength (Hu & Lazarian 2024a,b).

An example can be seen in Fig. 3, which compares synchrotron emission maps across different magnetic field strengths. For a strong magnetic field case ($\beta = 100$), the synchrotron map displays many filamentary and spur-like small-scale structures, particularly prominent in the central regions of the cluster. Conversely, in a scenario with a weaker magnetic field ($\beta = 500$), such filamentary and spur-like structures are markedly less pro-

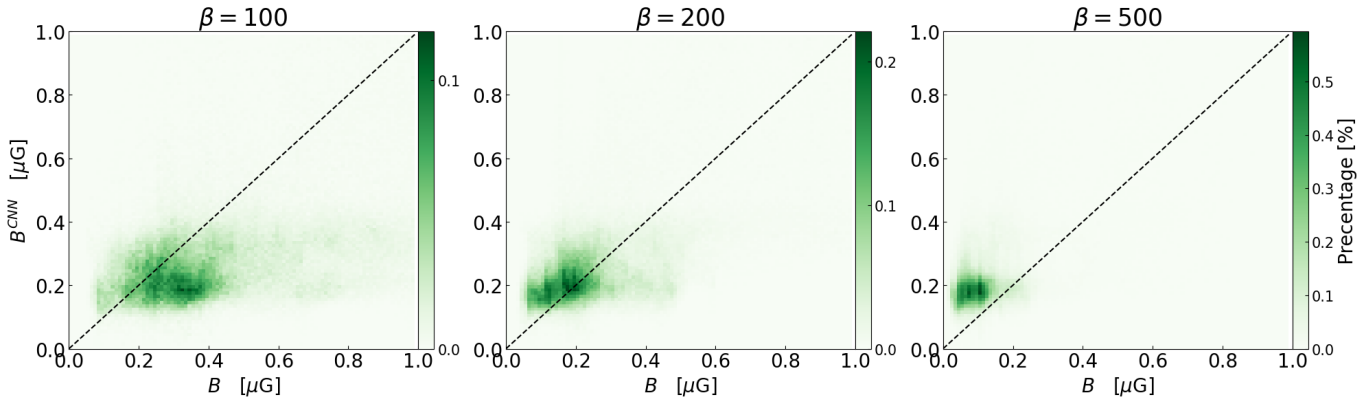

Figure 5. 2D histograms of the CNN-predicted magnetic field strength $B^{\rm CNN}$ and the corresponding actual density-weighted B. The three panels represent three physical conditions of $\beta = 100$ (left), $\beta = 200$ (middle), and $\beta = 300$ (right). The dashed diagonal line references the ideal scenario, where the predicted values match actual values.

nounced. This morphological difference underpins the rationale for employing a CNN model to predict magnetic field strength, as machine learning models are particularly adept at capturing and extracting these spatial features.

5.2. *CNN training and test using galaxy cluster simulations*

For training the CNN model, we utilized random cropping and rotation techniques to prepare the input data. Specifically, sub-fields of 16×16 pixels were randomly selected from synchrotron emission maps corresponding to three different magnetic field strengths ($\beta = 100, 200, 500$). For each training iteration, approximately 0.5 million sub-fields were used. The target for training was the density-weighted total magnetic field strength. We conducted 30 training iterations, continuing until the MSE loss function indicated saturation, suggesting that the model parameters had converged effectively. After training, the original synchrotron emission maps were used to test the accuracy of the CNN model. It is crucial to note that the randomly rotated images have different matrix representations compared to their originals. From CNN's perspective, these matrices represent distinct data points, potentially enhancing the model's robustness to orientation variations.

Fig. 4 shows a comparison between the CNN-predicted magnetic field strength and the actual mass-weighted magnetic field strength in the $\beta = 200$ simulation [2]. The actual magnetic field map is smoothed to match the resolution of the CNN prediction. Generally, they have an agreement on the center of galaxy clusters where most of the emission is concentrated., while locally, we notice differences in the cluster outskirts. In these regions, the magnetic fields are weak so we expect their role in shaping the synchrotron structure is not significant enough, so CNN prediction has more uncertainties.

Furthermore, Fig. 5 displays 2D histograms comparing the CNN predictions—$B^{\rm CNN}$—against the actual magnetic field strengths B derived from the simulations at $\beta = 100, 200$, and 500. These values span the typical magnetic field strength range observed in galaxy clusters (Carilli & Taylor 2002; Govoni & Feretti 2004). Despite some deviations, the predictions statistically correlate well with the actual magnetic field strengths, demonstrating the model's capability to estimate magnetic field strength based on synchrotron emission map.

5.3. *Effect of different view angles*

A remarkable challenge of galaxy observation is the observation angle. Galaxy clusters are not always face-on (see Fig. 3) and the projection effect could change the observed synchrotron emission and the projected magnetic field strength. Therefore, we introduced a certain rotation angle to the training data to evaluate the performance of the CNN model when the cluster is not face-on (i.e., rotation angle > 0 degrees). We rotate the simulation cubes with three separate angles, 30, 60, and 90 degrees, and repeat the CNN training.

Fig. 6 presents boxplots that quantify the deviations between the CNN-predicted values and the actual magnetic field strength. These deviations are quantified by calculating the absolute differences in the magnetic field strength distribution, $|B^{\rm CNN} - B|$, denoted as σ_B. After introducing rotation angles, we observe no significant changes in σ_B. The uncertainty ranges from 0.1μG to 1μG, with median values of σ_B approximately 0.22μG, 0.01μG, and 0.1μG for $\beta = 100$, 200, and 500 conditions, respectively. The CNN performs best for the $\beta = 500$ case, where the maximum uncertainty remains below

[2] The results of CNN-trained with turbulence simulations are given in Appendix A.

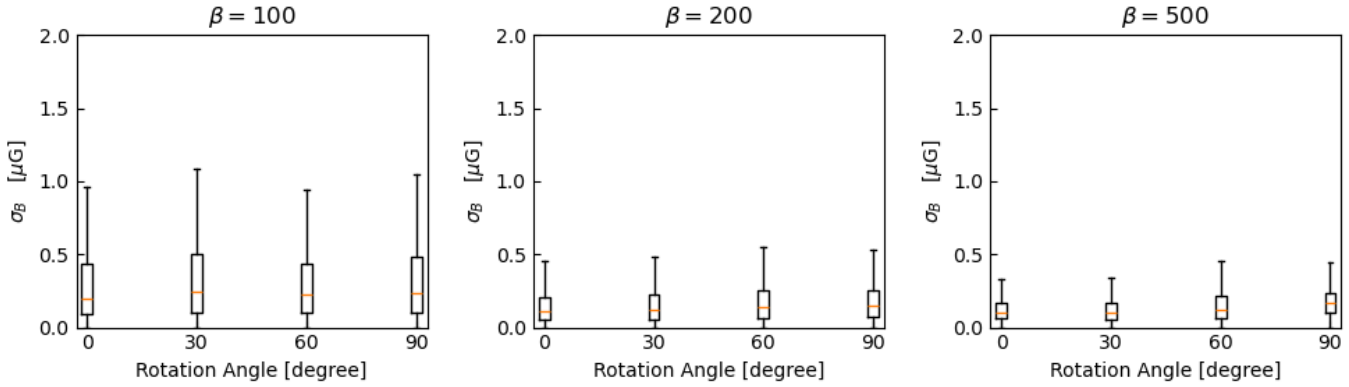

Figure 6. Boxplot of the errors of CNN model predictions with certain angle rotation in training data, i.e. $\beta = 100$ (left), $\beta = 200$ (middle), and $\beta = 500$ (right), and the corresponding rotation angle with 0, 30, 60, and 90 degrees.

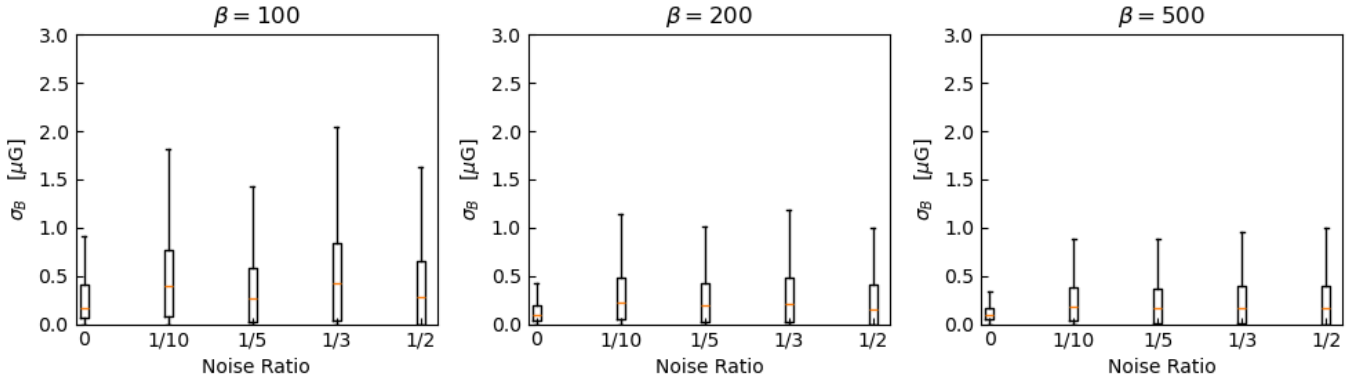

Figure 7. Boxplot of the errors of CNN model predictions with certain noise ratio in training data, i.e. $\beta = 100$ (left), $\beta = 200$ (middle), and $\beta = 500$ (right), and the corresponding noise ratio with 0, 1/10, 1/5, 1/3, and 1/2.

0.5μG. Overall, the CNN model's efficiency in predicting magnetic field strength appears to be largely insensitive to variations in view angles.

5.4. *Noise Effect*

Noise is an unavoidable aspect of observational data that can potentially influence the predictions made by CNN models. To assess this effect thoroughly, we introduced Gaussian noise into the synchrotron intensity maps utilized for training our CNN. The amplitude of the noise was varied to represent 1%, 20%, 33.3%, and 50% of the mean intensity of the maps, corresponding to the Noise Ratio(NR) of 1/10, 1/5, 1/3, and 1/2 respectively.

Fig. 7 presents boxplots that illustrate the deviations between the CNN-predicted magnetic strengths and the actual values under these different noise conditions. In a noise-free environment, the median values of σ_B are approximately 0.1μG. With the introduction of noise, the uncertainties in predictions increase significantly. The median values of σ_B rise to approximately 1μG for an NR of 1/2, 0.5μG for an NR of 1/5, and 0.3μG for an NR of 1/10. The increase in uncertainties correlates consistently with the intensity of the noise, demonstrating that higher levels of noise lead to greater prediction errors. Notably, the maximum uncertainties also escalate with stronger noise levels, indicating that the model's predictive accuracy deteriorates under high noise conditions. We also conducted tests with NR$\geq$ 1/2; however, at these extremely high NR levels, the magnetic field information was almost completely obscured by noise, making it impossible to make reliable predictions.

5.5. *Comparison with the equipartition magnetic field strength*

To estimate the magnetic field strength using radio observation, an equipartition between magnetic fields and cosmic rays is assumed. However, recent studies have also raised concerns about the validity of the equipartition condition (Beck & Krause 2005; Seta & Beck 2019; Ponnada et al. 2024). Both observational evidence and theoretical estimates suggest that it is difficult to reach equipartition between magnetic fields and cosmic ray electrons in galaxy clusters, as cosmic ray electrons get

cool rapidly and are often expected to have lower energy in these environments (Stepanov et al. 2014; Heesen et al. 2023; Ponnada et al. 2024). Accurately estimating the degree of non-equipartition remains challenging. By comparing traditional methods with CNN-based approaches, we can better quantify the degree of non-equipartition in galaxy clusters—a crucial factor in understanding the history and evolution of cosmic ray acceleration.

We make a comparison of the equipartition method and the CNN-based approach to measure magnetic field strength. This method assumes the energy in magnetic fields is $U_B \propto B^2$, the energy in relativistic particles is $U_{part} = U_{el} + U_{pr} \propto B^{-3/2}$. The total energy content U_{tot} is minimum when the contributions of magnetic fields and relativistic particles are approximately equal (equipartition condition). The corresponding magnetic field is commonly referred to as equipartition value $B_{\rm eq}$. Here we adopt the revised equipartition equation given by Beck & Krause (2005), in which $B_{\rm eq}$ is given by:

$$B_{\rm eq} = \left(\frac{4\pi(2\alpha+1)(1+\mathbf{K}_0)I_\nu E_p^{1-2\alpha}(\frac{\nu}{2C_1})^\alpha}{(2\alpha-1)C_2 l C_4}\right)^{1/(\alpha+3)}, \tag{10}$$

where $\alpha = (\gamma-1)/2$ and γ is the injection spectral index of the energy spectrum. l represents the integration pathlength and $E_p = 938.28$ Mev is the pectral break energy for protons. $C_1 = 6.26\times10^{18}{\rm erg^{-2}s^{-1}G^{-1}}, C_3 = C_3(\gamma+7/3)/(\gamma+1)\Gamma[(3\gamma-1)/12]\times\Gamma[(3\gamma+7)/12)], C_3 = 1.86\times10^{-23}$ erg G^{-1} sterad^{-1} are constants. $\mathbf{K}_0 = n_{p.0}/n_{e,0}$ refers to the number densities ratio of cosmic ray protons and electrons per particle energy interval within the energy range. I_ν is the synchrotron intensity given by:

$$I_v = \int dz\ C_2 N_0 E_0^\gamma (\frac{\nu}{2C_1})^{(1-\gamma)/2} B^{(1+\gamma)/2} C_4, \tag{11}$$

where $C_4 = (2/3)^{(\gamma+1)/4}$ accounts for the projection of total magnetic field strength to POS magnetic field strength. Compared with the classical equipartition equation, the revised method considers a particular energy limit E_p, referring to the point where state function for sub-relativistic cosmic ray electrons and photons becomes flattened due to ionization and/or Coulomb loss, resulting in a piece-wise particle density function (Pohl 1993).

In our calculations, we assume a frequency of $\nu = 1$ GHz and consider values of $\mathbf{K}_0 = 10$ and $\mathbf{K}_0 = 100$. Fig. 8 presents 2D histograms that compare the revised equipartition magnetic field strength, $B_{\rm eq}$, with the actual total magnetic field strength, B. The results show that $B_{\rm eq}$ is highly sensitive to the assumed value of $\mathbf{K}_0$, which represents the ratio of cosmic ray proton to electron number densities. A larger $\mathbf{K}_0$ implies that less energy is allocated to electrons, necessitating a stronger magnetic field to achieve the same level of synchrotron emission. Consequently, $B_{\rm eq}$ tends to overestimate the magnetic field strength when $\mathbf{K}_0$ is large, while a smaller $\mathbf{K}_0$ can lead to an underestimation.

In comparison to the CNN methodology, $\mathbf{K}_0$ is a critical yet challenging parameter to accurately estimate in observational data when using the equipartition method. The CNN approach, on the other hand, relies solely on the morphological differences in synchrotron emissions, enabling us to estimate the electron-to-proton ratio by comparing the CNN-predicted magnetic field with $B_{\rm eq}$.

6. DISCUSSION

6.1. *Prospects of the CNN-predicted magnetic field strength*

Understanding the magnetic field within galaxy clusters is crucial for addressing fundamental questions concerning cosmic ray acceleration mechanisms, the amplification of magnetic fields by turbulent dynamos, and the properties of dark matter candidates such as axion-like particles.

Building on the insights that the morphology of observed synchrotron structures encodes information about magnetic field strength (Hu & Lazarian 2024a,b), we propose utilizing Convolutional Neural Networks (CNNs) to extract these morphological features from synchrotron emissions and estimate magnetic field strengths in galaxy clusters. This approach is viable across different types of galaxy clusters, provided that suitable training datasets are available.

6.1.1. *Cosmic ray acceleration and transport*

An accurate characterization of magnetic field properties is essential for understanding the physics of cosmic rays (CRs). For example, mechanisms such as diffuse shock acceleration (Bell 1978b; Achterberg 2000; Brunetti & Jones 2014; Xu & Lazarian 2022) and turbulent second-order Fermi acceleration (Brunetti et al. 2001; Brunetti & Jones 2014) are widely recognized for their roles in CR acceleration within galaxy clusters. Both the strength and orientation of magnetic fields are critical factors influencing acceleration efficiency. Additionally, the diffusion coefficients for CRs, which are correlated with the medium's magnetization level, are influenced by the characteristics of turbulent magnetic fields (Yan & Lazarian 2008; Xu & Yan 2013; Hu et al. 2022b). The magnetic field strengths measured by CNNs can provide pivotal insights into the acceleration and transport processes of CRs

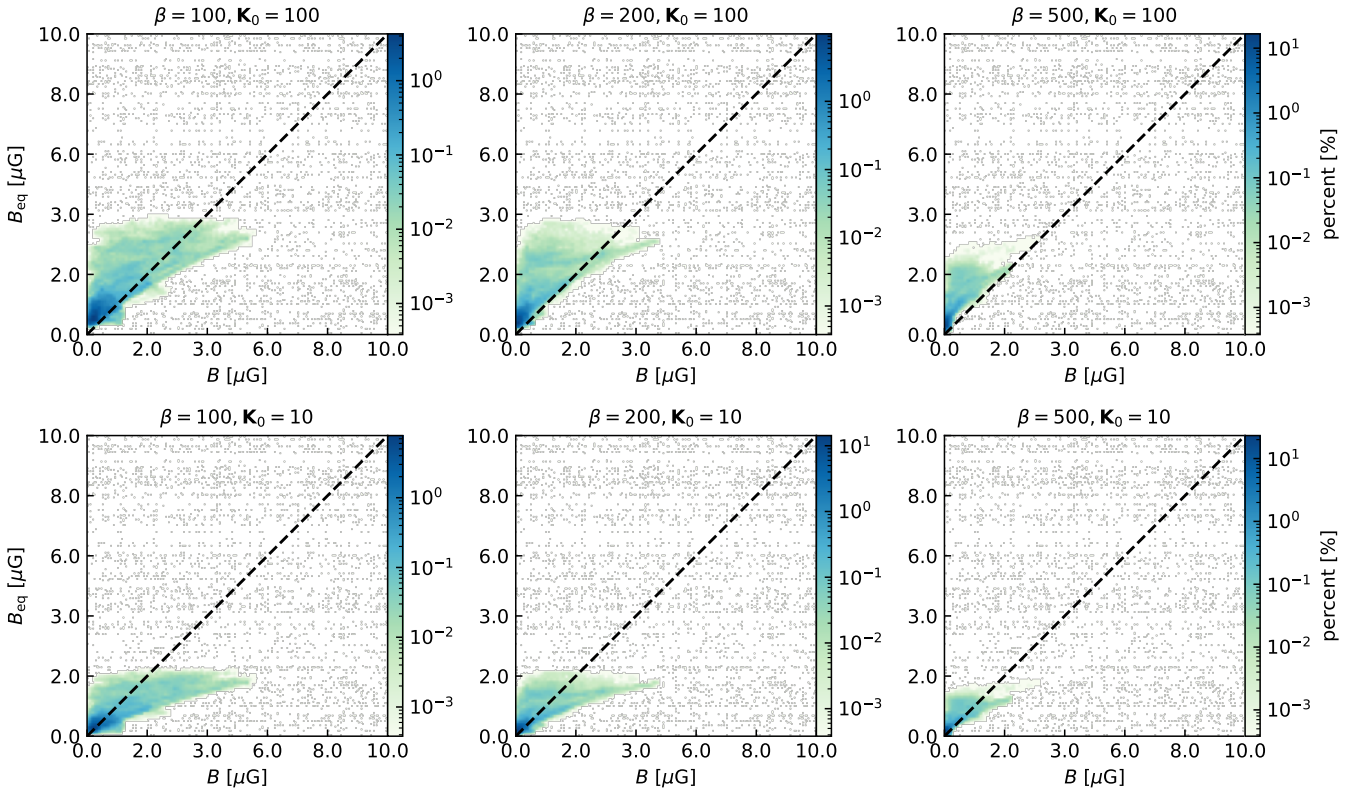

Figure 8. 2D histogram of the equipartition magnetic field strength $B_{\rm eq}$ and the corresponding actual density-weighted strength B. The dashed diagonal line references the ideal scenario, where the $B_{\rm eq}$ match B.

Moreover, the CNN approach does not presuppose equipartition between accelerated electrons and magnetic fields; it relies solely on the morphology of synchrotron emissions. Comparing the magnetic field strengths derived from equipartition and those predicted by CNNs offers a way to further constrain the relativistic electron number density and to explore the energy distribution among electrons, protons, and magnetic fields (see Fig. 8).

6.1.2. *Magnetic field amplification*

Magnetic field amplification during galactic mergers remains poorly understood. Previous numerical studies (Roettiger et al. 1999; Takizawa 2008; Donnert et al. 2018; Vazza et al. 2018) have suggested that magnetic fields evolve in concert with cluster dynamics: the fields are stretched and stirred, amplified by large-scale bulk flows along the merger axis. A small-scale turbulent dynamo further amplifies the magnetic field at subsequent stages. These predictions have been explored by earlier measurements from Rotation Measure grids (Murgia et al. 2004) and measurements of magnetic field orientation via synchrotron intensity gradients (Hu et al. 2024b). Our CNN methodology offers new perspectives for mapping the magnetic field strength within clusters, facilitating a detailed comparison between the numerical predictions of merging clusters and observational data.

6.1.3. *Cosmology: constrain axion-like particles*

Axion-like particles (ALPs) are a class of pseudoscalar particles that can generically couple to photons, making the oscillations between photons and ALPs in the presence of external magnetic fields possible (Wouters & Brun 2013). Efforts have been made to explore ALP parameters, particularly within the context of the Perseus cluster (Libanov & Troitsky 2020). Knowledge of magnetic field orientation and strength is crucial for placing stringent constraints on ALP parameters.

6.2. *Comparison with earlier work*

The exploration of magnetic fields using CNNs is advancing rapidly. Hu et al. (2024a) initially introduced a CNN model designed to estimate the 3D structure of magnetic fields, including the orientation of the POS magnetic field, the inclination angle, and the magnetization level of the medium in molecular clouds. Subsequently, Hu & Lazarian (2024a) extended this approach to synchrotron emission observations to trace the 3D magnetic field.

Previous studies primarily focused on estimating the medium's magnetization rather than the magnetic field strength itself. Building upon this foundation, our study expands the application of CNNs to the latter objective, utilizing synchrotron emission observations. Our CNN model is trained using MHD simulations of galaxy clusters, incorporating complex physical processes such as cluster mergers and sloshing motions. We demonstrate the CNN's capability to process these complicates and estimate magnetic field strengths.

6.3. *Uncertainty*

The training of the CNN model in this study relies on MHD simulations of turbulence or galaxy cluster mergers. To generate synthetic synchrotron observations, we assumed a uniform spectral index. In practice, however, the spectral index may vary across synchrotron emission maps, as electrons in different regions may undergo distinct acceleration and cooling processes. Variations in electron density distribution could alter the morphology of synchrotron structures. Despite these complexities, we anticipate that the CNN model will be able to identify correlations with magnetic field strength as more detailed synchrotron emission simulations become available for training.

7. CONCLUSION

In this study, we present a method that utilizes Convolutional Neural Networks (CNNs) in conjunction with synchrotron emission observations to estimate the magnetic field strength in galaxy clusters. The CNN approach leverages the distinctive features of magnetic field variations within observed synchrotron structures, offering a novel technique for extracting these variations. Our key findings are summarized as follows:

1. We designed and implemented a CNN model capable of extracting magnetic field strength from synchrotron emission maps across various physical conditions in galaxy clusters.

2. By training the model on MHD simulations of galaxy cluster mergers, we found that the median uncertainties for the CNN-estimated magnetic field strength are approximately 0.22μG, 0.01μG, and 0.1μG for $\beta = 100$, 200, and 500 conditions, respectively.

3. The model's robustness against noise and varying viewing angles was assessed, demonstrating that, with sufficient training, it is largely insensitive to these factors, ensuring reliable performance under a wide range of observational conditions.

4. We compared the magnetic field strengths estimated by the CNN with those derived using the equipartition method. Our CNN approach, which does not rely on equipartition assumptions, provides new insights into the constraints on relativistic electron number density and cosmic ray acceleration mechanisms.

Y.H. acknowledges the support for this work provided by NASA through the NASA Hubble Fellowship grant No. HST-HF2-51557.001 awarded by the Space Telescope Science Institute, which is operated by the Association of Universities for Research in Astronomy, Incorporated, under NASA contract NAS5-26555. A.L. acknowledges the support of NSF grants AST 2307840 and ALMA SOSPADA-016. This work used SDSC Expanse CPU, NCSA Delta CPU, and NCSA Delta GPU through allocations PHY230032, PHY230033, PHY230091, PHY230105, and PHY240183 from the Advanced Cyberinfrastructure Coordination Ecosystem: Services & Support (ACCESS) program, which is supported by National Science Foundation grants #2138259, #2138286, #2138307, #2137603, and #2138296.

Software: Python3 (Van Rossum & Drake 2009); TensorFlow (Abadi et al. 2015)

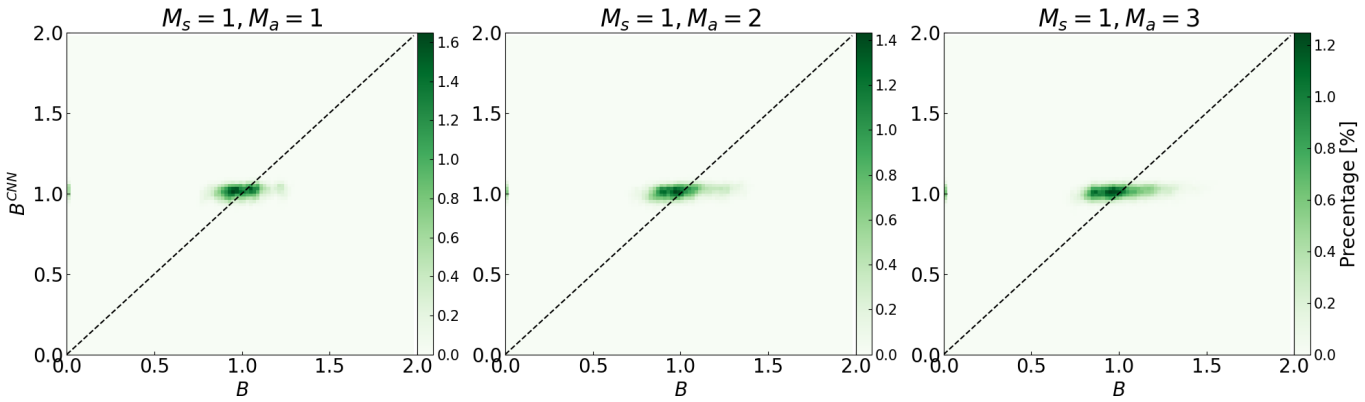

Figure 9. 2D histograms of the CNN-predicted normalized magnetic field strength $B^{\rm CNN}$ and the corresponding actual normalized density-weighted B. The magnetic field strength is normalized by the global mean value. The three panels represent three physical conditions of $M_s = 1, M_A = 1$ (left), $M_s = 1, M_A = 2$ (middle), and $M_s = 1, M_A = 3$ (right). The dashed diagonal line references the ideal scenario, where the predicted values match actual values.

APPENDIX

A. CNN TRAINING AND TEST USING MHD TURBULENCE SIMULATIONS

We test the CNN model's performance in estimating the magnetic field strength using MHD turbulence simulations. The MHD turbulence simulations were generated from the AthenaK code (Hu et al. 2024c; Stone et al. 2024). We solve the ideal MHD equations within an Eulerian framework, complemented by isothermal and periodic boundary conditions. Kinetic energy is solenoidally injected at wavenumber 2 to get a Kolmogorov-like power spectrum. The computational domain was discretized into a 792^3 cell grid, with numerical dissipation of turbulence occurring at scales between approximately 10 to 20 cells. Initial conditions for the simulations featured a uniform density field and a uniform magnetic field. Characterization of the scale-free turbulence within the simulations was achieved through M_s and M_A. To explore the physical conditions of galaxy clusters, we use $M_s \approx 1$ and $M_A \approx 1, 2, 3, 4$, and 5, corresponding to $\beta = 2, 8, 18, 32$, and 50, respectively.

Fig. 9 presents 2D histograms comparing CNN predictions with actual magnetic field strengths derived from simulations with $M_A \approx 1, 2$, and 3. The CNN predictions show a strong statistical correlation with the true magnetic field strengths, especially when normalized magnetic strength is considered instead of the absolute value. This indicates the potential of estimating magnetic field strength based on synchrotron emission maps.

REFERENCES

Abadi, M., Agarwal, A., Barham, P., et al. 2015, TensorFlow: Large-Scale Machine Learning on Heterogeneous Systems. https://www.tensorflow.org/

Achterberg, A. 2000, in Highly Energetic Physical Processes and Mechanisms for Emission from Astrophysical Plasmas, ed. P. C. H. Martens, S. Tsuruta, & M. A. Weber, Vol. 195, 291

Alina, D., Montillaud, J., Hu, Y., et al. 2022, A&A, 658, A90, doi: 10.1051/0004-6361/202039065

Andrecut, M., Stil, J., & Taylor, A. 2011, The Astronomical Journal, 143, 33

Arshakian, T. G., Beck, R., Krause, M., & Sokoloff, D. 2009, A&A, 494, 21, doi: 10.1051/0004-6361:200810964

Beck, R., & Krause, M. 2005, Astronomische Nachrichten, 326, 414, doi: 10.1002/asna.200510366

Bell, A. R. 1978a, MNRAS, 182, 443, doi: 10.1093/mnras/182.3.443

—. 1978b, MNRAS, 182, 147, doi: 10.1093/mnras/182.2.147

—. 2004, MNRAS, 353, 550, doi: 10.1111/j.1365-2966.2004.08097.x

Bonafede, A., Intema, H. T., Brüggen, M., et al. 2014, ApJ, 785, 1, doi: 10.1088/0004-637X/785/1/1

Brentjens, M. A., & De Bruyn, A. 2005, Astronomy & Astrophysics, 441, 1217

Brunetti, G., & Jones, T. W. 2014, International Journal of Modern Physics D, 23, 1430007, doi: 10.1142/S0218271814300079

Brunetti, G., Setti, G., Feretti, L., & Giovannini, G. 2001, MNRAS, 320, 365, doi: 10.1046/j.1365-8711.2001.03978.x

Burkhart, B., & Mocz, P. 2019, ApJ, 879, 129, doi: 10.3847/1538-4357/ab25ed

Bykov, A. M., Ellison, D. C., & Renaud, M. 2012, SSRv, 166, 71, doi: 10.1007/s11214-011-9761-4

Caprioli, D., & Spitkovsky, A. 2014, ApJ, 783, 91, doi: 10.1088/0004-637X/783/2/91

Carilli, C. L., & Taylor, G. B. 2002, ARA&A, 40, 319, doi: 10.1146/annurev.astro.40.060401.093852

Chevalier, R. A., & Luo, D. 1994, ApJ, 421, 225, doi: 10.1086/173640

Condon, J. 1992, Annual review of astronomy and astrophysics, 30, 575

Donnert, J., Vazza, F., Brüggen, M., & ZuHone, J. 2018, SSRv, 214, 122, doi: 10.1007/s11214-018-0556-8

Dubey, A., Antypas, K., Ganapathy, M. K., et al. 2009, Parallel Computing, 35, 512

Evans, C. R., & Hawley, J. F. 1988, Astrophysical Journal, Part 1 (ISSN 0004-637X), vol. 332, Sept. 15, 1988, p. 659-677., 332, 659

Federrath, C., & Klessen, R. S. 2012, ApJ, 761, 156, doi: 10.1088/0004-637X/761/2/156

Fryxell, B., Olson, K., Ricker, P., et al. 2000, The Astrophysical Journal Supplement Series, 131, 273

Goldreich, P., & Sridhar, S. 1995, ApJ, 438, 763, doi: 10.1086/175121

Govoni, F., & Feretti, L. 2004, International Journal of Modern Physics D, 13, 1549, doi: 10.1142/S0218271804005080

Heesen, V., Klocke, T.-L., Brüggen, M., et al. 2023, Astronomy & Astrophysics, 669, A8

Hu, Y., & Lazarian, A. 2023, MNRAS, 524, 4431, doi: 10.1093/mnras/stad2158

—. 2024a, ApJ, 975, 66, doi: 10.3847/1538-4357/ad7950

—. 2024b, arXiv e-prints, arXiv:2410.09294, doi: 10.48550/arXiv.2410.09294

Hu, Y., Lazarian, A., Beck, R., & Xu, S. 2022a, ApJ, 941, 92, doi: 10.3847/1538-4357/ac9df0

Hu, Y., Lazarian, A., & Stanimirović, S. 2021, ApJ, 912, 2, doi: 10.3847/1538-4357/abedb7

Hu, Y., Lazarian, A., Wu, Y., & Fu, C. 2024a, MNRAS, 527, 11240, doi: 10.1093/mnras/stad3766

Hu, Y., Lazarian, A., & Xu, S. 2022b, MNRAS, 512, 2111, doi: 10.1093/mnras/stac319

Hu, Y., Stuardi, C., Lazarian, A., et al. 2024b, Nature Communications, 15, 1006, doi: 10.1038/s41467-024-45164-8

Hu, Y., Xu, S., Arzamasskiy, L., Stone, J. M., & Lazarian, A. 2024c, MNRAS, 527, 3945, doi: 10.1093/mnras/stad3493

Ioffe, S., & Szegedy, C. 2015, in International conference on machine learning, pmlr, 448–456

Johnson, A. R., Rudnick, L., Jones, T. W., Mendygral, P. J., & Dolag, K. 2020, ApJ, 888, 101, doi: 10.3847/1538-4357/ab5d30

Jokipii, J. R. 1966, ApJ, 146, 480, doi: 10.1086/148912

Larochelle, H., Erhan, D., Courville, A., Bergstra, J., & Bengio, Y. 2007, in Proceedings of the 24th international conference on Machine learning, ICML '07 & ILP '07 (ACM), doi: 10.1145/1273496.1273556

Lazarian, A. 2006, ApJL, 645, L25, doi: 10.1086/505796

Lazarian, A., Esquivel, A., & Crutcher, R. 2012, ApJ, 757, 154, doi: 10.1088/0004-637X/757/2/154

Lazarian, A., & Pogosyan, D. 2012, ApJ, 747, 5, doi: 10.1088/0004-637X/747/1/5

Lazarian, A., & Vishniac, E. T. 1999, ApJ, 517, 700, doi: 10.1086/307233

Lazarian, A., Yuen, K. H., & Pogosyan, D. 2022, ApJ, 935, 77, doi: 10.3847/1538-4357/ac6877

—. 2024, ApJ, 974, 237, doi: 10.3847/1538-4357/ad6d62

LeCun, Y., Bottou, L., Bengio, Y., & Haffner, P. 1998, Proceedings of the IEEE, 86, 2278

Lee, H., Lazarian, A., & Cho, J. 2016, ApJ, 831, 77, doi: 10.3847/0004-637X/831/1/77

Libanov, M., & Troitsky, S. 2020, Physics Letters B, 802, 135252, doi: 10.1016/j.physletb.2020.135252

Mac Low, M.-M., & Klessen, R. S. 2004, Reviews of Modern Physics, 76, 125, doi: 10.1103/RevModPhys.76.125

McKee, C. F., & Ostriker, E. C. 2007, ARA&A, 45, 565, doi: 10.1146/annurev.astro.45.051806.110602

Melrose, D. 2010, The Astrophysical Journal, 725, 1600

Mestel, L. 1965, QJRAS, 6, 265

Murgia, M., Govoni, F., Feretti, L., et al. 2004, Astronomy & Astrophysics, 424, 429

Murgia, M., Govoni, F., Feretti, L., et al. 2004, A&A, 424, 429, doi: 10.1051/0004-6361:20040191

Nipoti, C., Posti, L., Ettori, S., & Bianconi, M. 2015, Journal of Plasma Physics, 81, 495810508, doi: 10.1017/S0022377815000781

Pacholczyk, A. G. 1970, Radio astrophysics. Nonthermal processes in galactic and extragalactic sources

Perrone, L. M., & Latter, H. 2022, MNRAS, 513, 4625, doi: 10.1093/mnras/stac975

Planck Collaboration, Adam, R., Ade, P. A. R., et al. 2016, A&A, 594, A10, doi: 10.1051/0004-6361/201525967

Pohl, M. 1993, Astronomy and Astrophysics (ISSN 0004-6361), vol. 270, no. 1-2, p. 91-101., 270, 91

Ponnada, S. B., Panopoulou, G. V., Butsky, I. S., et al. 2024, MNRAS, 527, 11707, doi: 10.1093/mnras/stad3978

Roettiger, K., Stone, J. M., & Burns, J. O. 1999, ApJ, 518, 594, doi: 10.1086/307298

Rumelhart, D. E., Hinton, G. E., & Williams, R. J. 1986, nature, 323, 533

Rybicki, G. B., & Lightman, A. P. 1986, Radiative Processes in Astrophysics

Scherer, D., Müller, A., & Behnke, S. 2010, in International conference on artificial neural networks, Springer, 92–101

Schmaltz, T., Hu, Y., & Lazarian, A. 2024, submitted to ApJ

Seta, A., & Beck, R. 2019, Galaxies, 7, 45

Stepanov, R., Shukurov, A., Fletcher, A., et al. 2014, Monthly Notices of the Royal Astronomical Society, 437, 2201

Stone, J. M., Mullen, P. D., Fielding, D., et al. 2024, arXiv e-prints, arXiv:2409.16053, doi: 10.48550/arXiv.2409.16053

Stuardi, C., Bonafede, A., Lovisari, L., et al. 2021, MNRAS, 502, 2518, doi: 10.1093/mnras/stab218

Takahashi, R., Matsubara, T., & Uehara, K. 2020, IEEE Transactions on Circuits and Systems for Video Technology, 30, 2917–2931, doi: 10.1109/tcsvt.2019.2935128

Takizawa, M. 2008, ApJ, 687, 951, doi: 10.1086/592059

van Dyk, D. A., & Meng, X.-L. 2001, Journal of Computational and Graphical Statistics, 10, 1–50, doi: 10.1198/10618600152418584

Van Rossum, G., & Drake, F. L. 2009, Python 3 Reference Manual (Scotts Valley, CA: CreateSpace)

Vazza, F., Brunetti, G., Brüggen, M., & Bonafede, A. 2018, MNRAS, 474, 1672, doi: 10.1093/mnras/stx2830

Wouters, D., & Brun, P. 2013, ApJ, 772, 44, doi: 10.1088/0004-637X/772/1/44

Xu, S. 2019, Study on Magnetohydrodynamic Turbulence and Its Astrophysical Applications, Springer Theses (Springer Nature Singapore). https://books.google.com/books?id=oXWUDwAAQBAJ

Xu, S. 2022, ApJ, 934, 136, doi: 10.3847/1538-4357/ac7c68

Xu, S., & Lazarian, A. 2022, ApJ, 925, 48, doi: 10.3847/1538-4357/ac3824

Xu, S., & Yan, H. 2013, ApJ, 779, 140, doi: 10.1088/0004-637X/779/2/140

Yan, H., & Lazarian, A. 2002, PhRvL, 89, 281102, doi: 10.1103/PhysRevLett.89.281102

—. 2008, ApJ, 673, 942, doi: 10.1086/524771

Zhang, J.-F., Lazarian, A., Ho, K. W., et al. 2019a, MNRAS, 486, 4813, doi: 10.1093/mnras/stz1176

Zhang, J.-F., Liu, Q., & Lazarian, A. 2019b, ApJ, 886, 63, doi: 10.3847/1538-4357/ab4b4a

ZuHone, J. A., Kowalik, K., Öhman, E., Lau, E., & Nagai, D. 2018, ApJS, 234, 4, doi: 10.3847/1538-4365/aa99db

ZuHone, J. A., Markevitch, M., & Lee, D. 2011, ApJ, 743, 16, doi: 10.1088/0004-637X/743/1/16